8 June 2007 | $10

Science

AAAS

Evolution and Development of Inflorescence Architectures

Przemyslaw Prusinkiewicz,[1] Yvette Erasmus,[2]* Brendan Lane,[1]
Lawrence D. Harder,[3] Enrico Coen[2]†

To understand the constraints on biological diversity, we analyzed how selection and development interact to control the evolution of inflorescences, the branching structures that bear flowers. We show that a single developmental model accounts for the restricted range of inflorescence types observed in nature and that this model is supported by molecular genetic studies. The model predicts associations between inflorescence architecture, climate, and life history, which we validated empirically. Paths, or evolutionary wormholes, link different architectures in a multidimensional fitness space, but the rate of evolution along these paths is constrained by genetic and environmental factors, which explains why some evolutionary transitions are rare between closely related plant taxa.

Organisms display great diversity in shape and architecture, but the range of observed forms represents only a small fraction of what is theoretically possible (*1*, *2*). For example, when patterns of shell coiling are considered within a mathematically defined space of possible forms (morphospace), the observed forms are restricted to only a subregion of this space (*3*). One explanation for such restrictions is selection (*4*). However, it is likely that developmental and genetic mechanisms also play a role. For example, the absence of vertebrates with more than four limbs is thought to reflect an interplay between both developmental and selective constraints (*5*, *6*). Developmental mechanisms restrict the range of genetic and phenotypic variation available for selection, whereas selection influences the evolution of developmental processes. Such two-way interactions can be unravelled using morphospaces based on developmental genetic mechanisms. We take this approach for the evolution of inflorescences, which has a history of both theoretical and molecular genetic analysis.

The arrangement of flowers on a plant reflects an iterative pattern of developmental decisions at the growing tips, or meristems. Each iteration occurs over a time interval known as a plastochron (*7*), during which a meristem may either switch to floral identity or continue to produce further meristems and, hence, branches. As the number of iterations rises, the number of theoretically possible structures increases rapidly (*8*). However, only a small subset of these structures corresponds to inflorescences observed in nature (Fig. 1). They are grouped into three broad architectural types: (i) panicles, which comprise a branching series of axes that terminate in flowers; (ii) racemes, which comprise axes bearing flowers in lateral positions or lateral axes that reiterate this pattern; and (iii) cymes, which comprise axes that terminate in flowers and lateral axes that reiterate this pattern (*9*–*11*) (Fig. 1, D to I). The appearance of each inflorescence type varies according to the arrangement of lateral meristems around the stem (phyllotaxy), the pattern of internode lengths, and additional variations on the three architectural themes. Although panicles, racemes, and cymes are all found among flowering plants, a restricted range of types is evident at local taxonomic levels: Genera seldom include species with both racemes and cymes.

These observations raise two related questions. First, what determines the extent of morphospace occupied by inflorescences in nature: Why do we find these three main architectural types and not more or fewer? Second, what constrains evolution within the occupied morphospace, imposing a local barrier between racemes and cymes?

A unifying inflorescence model. Previously, distinct developmental models have been postulated for different inflorescence types (*12*, *13*), leading to a fractured view of phenotypic space. From an evolutionary perspective, however, inflorescence types should be related to each other through genetic changes. A developmental model that encompasses different architectural types within a single parameter space is thus needed. To construct it, we considered meristems giving rise to shoots or flowers as two extremes of a continuum. The variable that characterizes this continuum is called vegetativeness (*veg*), with high levels of *veg* corresponding to shoot meristem identity and low levels to flower meristem identity. The *veg* level may be related to many factors such as plant age, meristem position, internal state of a meristem, and the environment (*14*–*17*). For simplicity, we identify the factors influencing *veg* as plant age *t*, measured from the beginning of inflorescence development, and/or the internal state of the meristem.

If *veg* is high and does not change with time, an indeterminate vegetative branching structure is generated (Fig. 2A). For the plant to produce flowers, *veg* must decline in some or all meristems during growth. The simplest assumption is that *veg* decreases in all meristems equally. The resulting architecture is a panicle of flowers, which form at time *T* when low levels of *veg* are reached (Fig. 2B).

To generate further architectural types, we assume that meristems can be in one of two internal states, A and B, such that meristems in these states attain low levels of *veg* at different

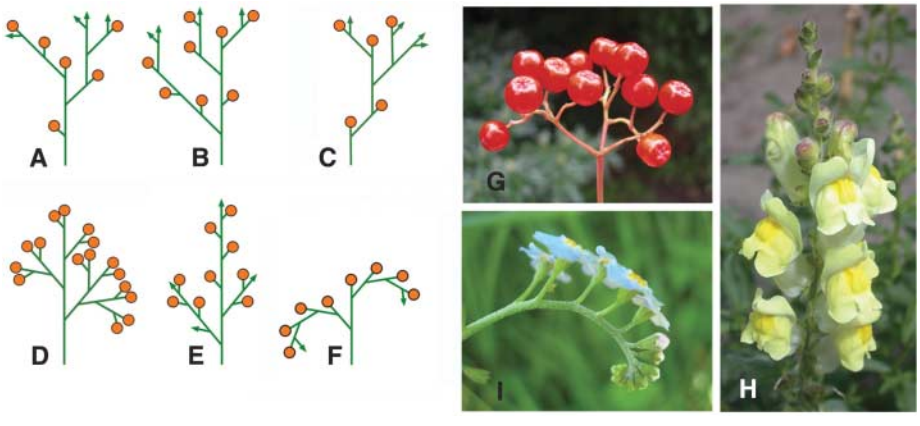

Fig. 1. Hypothetical and observed inflorescence structures. Arrows, meristems; circles, flowers. (**A** to **C**) Inflorescence structures not observed in nature. (**D** to **F**) Three main classes of inflorescence architectures: panicle (D), raceme (E), and cyme (F). (**G** to **I**) Species illustrating inflorescence types: (G) fruiting panicle of *Sorbus aucuparia*, (H) flowering raceme of *Antirrhinum majus,* (I) flowering cyme of *Myosotis arvensis*.

[1]Department of Computer Science, University of Calgary, 2500 University Drive N.W. Calgary, Alberta T2N 1N4, Canada. [2]Department of Cell and Developmental Biology, John Innes Centre, Colney Lane, Norwich NR4 7UH, UK. [3]Department of Biological Sciences, University of Calgary, 2500 University Drive N.W. Calgary, Alberta T2N 1N4, Canada.

*Present address: Institute of Molecular Plant Science, Daniel Rutherford Building, Kings Buildings, Mayfield Road, Edinburgh, EH9 3JR, UK.

†To whom correspondence should be addressed. Email: enrico.coen@bbsrc.ac.uk

times, T_A and T_B. Suppose that the apical meristem of the main axis is in state A, whereas all lateral meristems are in state B. If $T_B < T_A$, lateral meristems will attain floral identity more quickly than does the apical meristem, yielding a raceme in the upper part of the plant (red path in Fig. 2C). However, lateral apices in the lower part of the inflorescence will also rapidly progress toward floral identity, producing a graded series of panicles (orange path in Fig. 2C). This result is inconsistent with the structure of lateral branches of compound racemes, which typically do not terminate in flowers (Fig. 1E).

To resolve this discrepancy, we postulate that state B is transient. All lateral meristems are formed in state B, but they have two possible fates afterwards. If *veg* is sufficiently low, the meristem becomes a flower (red path, Fig. 2D). Otherwise, the meristem reverts to state A and produces a branch (orange path, Fig. 2D). The rationale for this reversion is that a newly created meristem (state B) changes its identity once it becomes the terminal meristem of the next-order branch (state A). Biologically, state B represents the stage when a meristem is newly formed (immature), whereas state A represents a more advanced stage of meristem development (mature). We call the resulting model the transient model.

A key feature of the transient model is that it can generate cymes as well as racemes and panicles, thus accounting for these inflorescence types within a single framework. In cymes, lateral meristems repetitively create meristems in two different states: a terminal meristem giving rise to a flower, and a lateral meristem giving rise to a branch (Fig. 1F). This can be captured with the transient model by setting $T_A < T_B$. Immature lateral meristems then take longer to attain floral identity than do mature meristems, creating the reverse of the situation for racemes (Fig. 2E).

The region of morphospace generated by the transient model is illustrated in Fig. 3. The main diagonal ($T_A = T_B$) corresponds to panicles, flanked by racemes on one side ($T_A > T_B$) and cymes on the other ($T_A < T_B$). This planar region represents only a slice of the entire morphospace. For example, the hypothetical forms shown in Fig. 1, A to C, do not lie in this region and could only be generated with more complex mechanisms. The transient mechanism may therefore account for the restriction of observed inflorescence types to a small region of morphospace. Potentially adaptive architectures may not be attained in nature because they cannot be produced by developmental processes captured by the transient mechanism.

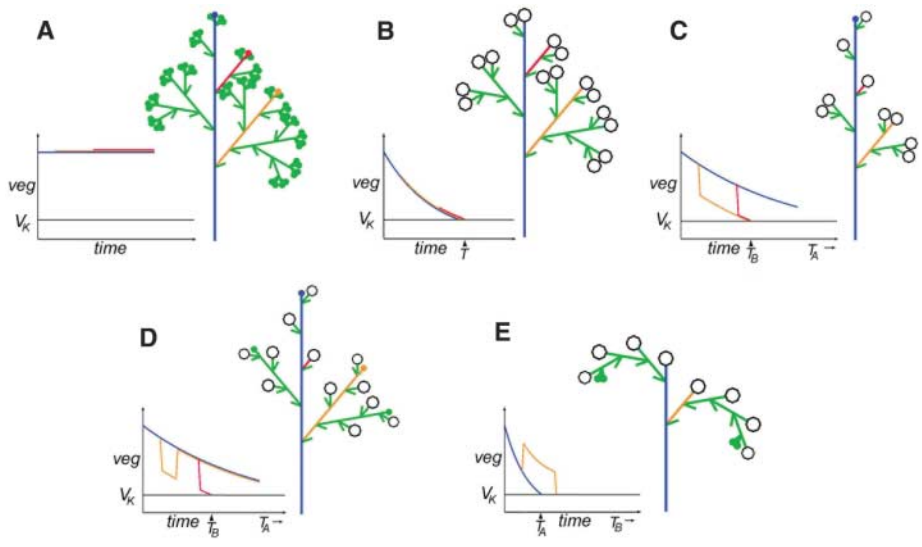

Fig. 2. Architectures and time course of *veg* decline for various inflorescence models. Small filled circles, meristems; white circles, flowers. Colors highlight paths of representative meristems: main meristem, blue; lowest lateral meristem, orange; third lateral meristem from bottom, red. Plots show the time course of *veg* decline in selected meristems after their initiation. (**A**) Level of *veg* does not change with time; an indeterminate vegetative branching structure results. (**B**) *Veg* declines at a similar rate in all meristems and yields flowers upon reaching threshold V_K at time T; a panicle results. (**C**) *Veg* in apical meristems (state A) reaches threshold V_K at time $T_A > T_B$ for lateral meristems (state B). The resulting structure is a compound raceme, with lower branches terminating in flowers. (**D**) Transient model in which lateral meristems are initially in state B but revert to state A if *veg* does not reach the threshold V_K; a raceme with indeterminate branches is produced for $T_B < T_A$. (**E**) Transient model in which $T_B > T_A$ yields a cyme.

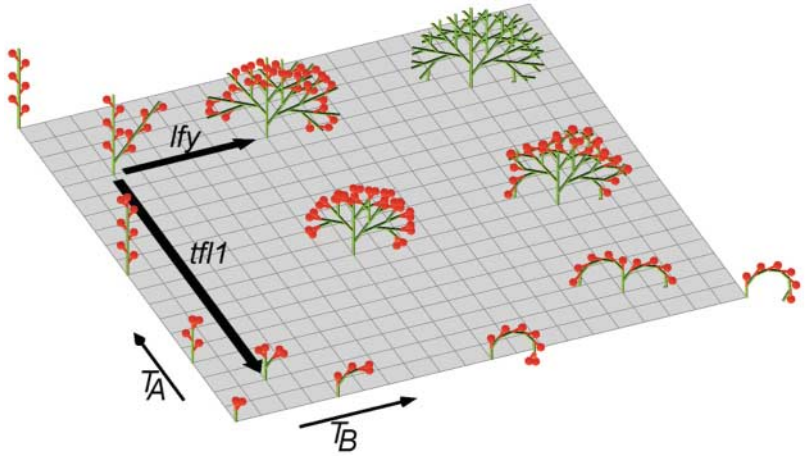

Fig. 3. Morphospace for the transient model. Different phenotypes are generated by varying the times T_A and T_B at which flowers begin to form. Values along each axis range from 0 to 10 plastochrons. Black arrows, pointing away from the wild-type architecture of *Arabidopsis*, indicate the effect of *tfl1* and *lfy* mutations [under inductive conditions (*20*)]. Inflorescences are shown at six plastochrons.

Integration of models with developmental and molecular genetics. To assess the plausibility of the transient model, we related it to underlying genetic mechanisms. We focused on two architectural genes from *Arabidopsis*, *TERMINAL FLOWER 1* (*TFL1*) and *LEAFY* (*LFY*) (*18*–*23*), as they produce phenotypes that displace the wild-type plant in orthogonal directions in morphospace (Fig. 3). Compared to wild-type *Arabidopsis,* which produces branched racemes, mutants lacking *TFL1* activity produce inflorescences with short axes that terminate in flowers, whereas mutants lacking *LFY* produce highly branched inflorescences bearing shootlike flowers.

We incorporated genes into the transient model by postulating that *TFL1* increases *veg* and *LFY* reduces *veg* in meristems (Fig. 4A). The wild-type *Arabidopsis* architecture results from high *TFL1* and low *LFY* activity in state A meristems (yielding high *veg*) and high *LFY* and low *TFL1* activity in state B meristems (yielding low *veg*). This pattern of gene expression is produced by assuming that: (i) *LFY* and *TFL1* inhibit each other (*18*, *20*, *22*), (ii) *TFL1* expression is inhibited in state B, (iii) *LFY* is less sensitive to *TFL1* inhibition in state B [this enhances *LFY* in B meristems and allows *LFY* to attain high activity even in plants overexpressing

TFL1 (*24*)], and (iv) the levels of *TFL1* and *LFY* increase with plant age (*21*, *25*). The shootlike flowers observed in *lfy* mutants (*20*) and plants overexpressing *TFL1* (*22*, *24*) are captured by assuming that they correspond to intermediate *veg* levels, lying between the levels for normal shoots and flowers.

With these assumptions, the transient model largely accounts for mutant and overexpression phenotypes of *Arabidopsis* (Fig. 4, B to H, and SOM text) and for observed patterns of gene expression. According to the model, a lateral meristem that gives rise to a branch is initially in state B, which corresponds to relatively low *TFL1* and high *LFY*. This pattern reverses when the meristem switches back to state A. These features agree with experimental data: *TFL1* expression is low in newly formed lateral primordia and only increases later (*22*). Furthermore, *LFY* is expressed early in primordia that will give rise to lateral branches but is absent from mature lateral shoot meristems (*25*, *26*). The transient model thus provides a functional explanation for observed expression patterns.

Evolutionary origins and implications of the transient mechanism. Both the range of architectural types observed in flowering plants and molecular genetic data lend support to the transient mechanism, but the evolutionary origin of this mechanism is unclear. To elucidate it, we

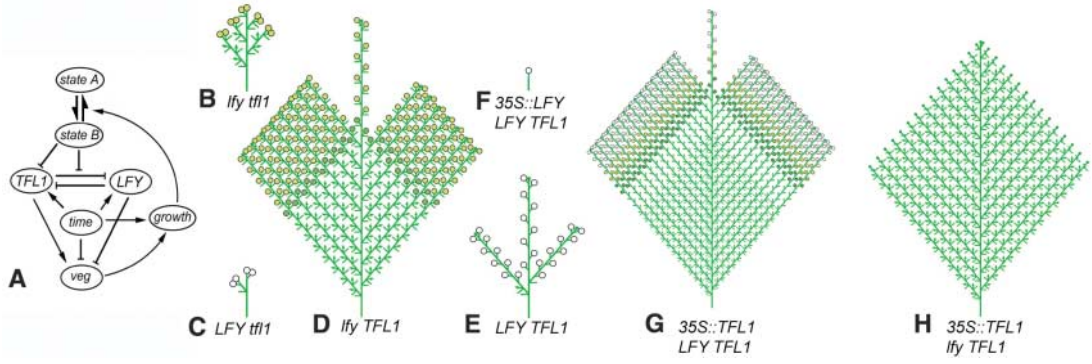

Fig. 4. Incorporating *LFY* and *TFL1* genes into the transient model for *Arabidopsis*. (**A**) Interactions between genes, time, *veg*, and growth underlying the model. Growth increases the number of modules and hence influences the spatial pattern of gene expression. Gene activity affects *veg* and hence influences whether a meristem will continue to generate more modules or whether it will cease growing. Arrowheads indicate up-regulation; bars, down-regulation. Growth promotes production of meristems in state A or B, with state B reverting to A unless the floral threshold is reached. (**B** to **H**) Wild-type, mutant, and transgenic phenotypes generated by the model with the interactions shown in (A), assuming inductive conditions (*20*). Circles indicate flowers, color-coded according to *veg* levels. White, normal flower; yellow/green, shootlike flower). Arrows indicate branches. (For detailed explanation, see SOM.)

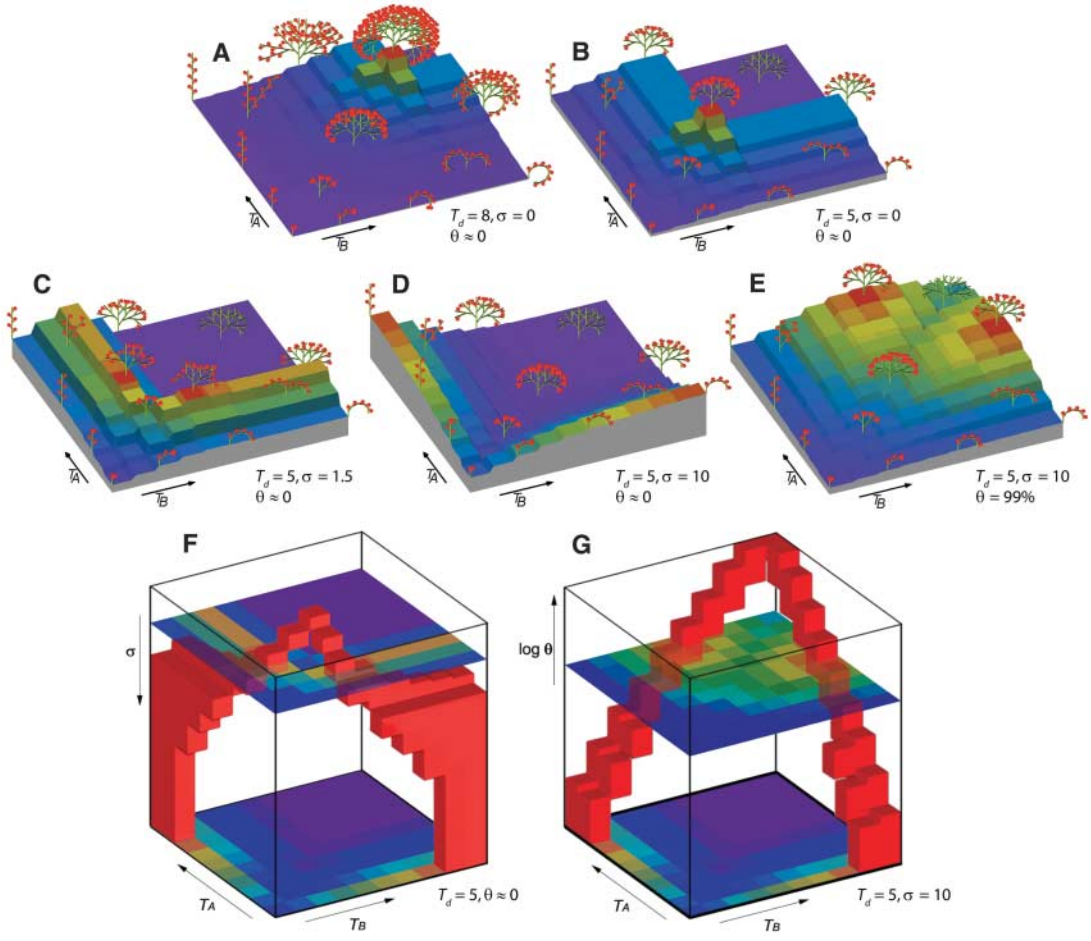

Fig. 5. (**A** to **E**) Two-dimensional fitness landscapes. Fitness levels are indicated by height and color. For each genotype, fitness is calculated over seasons with an average duration T_d and standard deviation σ, assuming that fraction θ of mature plants survives from one season to the next. Plants illustrate the architecture generated at time T_d. (A) For annuals with fixed growth duration, the optimal inflorescence is a panicle, represented by a single adaptive peak. (B) If T_d is reduced, the optimal architecture is a less highly branched panicle. (C) When σ is increased, two peaks arise corresponding to compound racemes and cymes. (D) With a further increase in σ, the peaks diverge. Optimal architectures are simple racemes and cymes. (E) Increased longevity θ shifts the peaks toward panicles. (**F** and **G**) Regions of high fitness in 3D fitness spaces. Horizontal sections correspond to the high-fitness regions in 2D fitness landscapes. (F) Path capturing the relation between architecture and σ. Colored sections correspond to figures (C) (top) and (D) (bottom). (G) Wormhole capturing the relation between architectures and longevity θ. Colored sections correspond to figures (D) (bottom) and (E) (top).

considered the fitness of different architectures in the region of morphospace generated by the transient model (SOM text).

With unlimited pollination and a growing season of fixed length, the optimal inflorescence architecture is a panicle. This is because the plant can delay flowering by keeping its meristems in a vegetative state until the latest time needed for fruit production, thus maximizing branching and the number of fruits (Fig. 5, A and B). However, if the length of the growth seasons varies from year to year, a plant that delays flowering too long may fail to produce any fruits by the end of a short season. This would reduce fitness, particularly if annual seed production is essential for genotype survival. The best strategy may thus be for a plant to "hedge its bets" (*27*–*32*) and generate flowers sequentially during a season, so that some flowers are produced early if the season is short but more flowers can still be produced later if the season is long. Racemes and cymes, in which only a fraction of meristems switch to floral identity at any time, may then have higher fitness values than panicles. This is illustrated in Fig. 5, C and D, in which racemes and cymes form separate adaptive peaks in the fitness landscape for annual plants, with the positions of the peaks depending on the standard deviation of growth duration.

To the extent that the impact of variable season length increases from tropical to more temperate conditions, our model predicts higher frequencies of racemes and cymes in temperate compared with tropical climates, and the opposite trend for panicles. To test these predictions, we extracted the incidence of each architectural type in different climatic zones from the Watson and Dallwitz database of angiosperm families (*33*) (fig. S1A). Although this database is not ideal for our purposes, as it aggregates characters for all species in the same family, it reveals significant trends. Consistent with our predictions, cymes are relatively more frequent in more temperate conditions ($P < 0.01$), whereas panicles show the opposite trend ($P < 0.001$). Racemes are also more frequent in temperate than tropical conditions, but not significantly ($P > 0.2$).

In addition to the environmental influences, positions of peaks in the theoretical fitness landscapes depend on factors under genetic control, such as plant longevity. If a plant is perennial (i.e., lives more than 1 year), the negative impact of short seasons in an uncertain environment is reduced by spreading the risk over multiple years (Fig. 5E). We found no significant associations of raceme or panicle architectures with longevity, but cymes are significantly less common in families with only woody perennials and more common in families with annuals, as predicted (fig. S1B) ($P < 0.05$). Furthermore, this trend is observed in temperate but not tropical families. Although we have focused on the effects of environmental uncertainty, similar theoretical fitness landscapes involving interactions between internal and external factors could also be generated by considering the effects of limitations on pollination rate.

Although these results provide a rationale for sequential patterns of flower production, they do not explain why the transient mechanism evolved rather than other developmental mechanisms. One possibility is that the transient mechanism arose more readily because it built on the preexisting developmental process of meristem establishment. Establishing a new lateral meristem requires a period of time during which genes needed for meristem maintenance become activated (*34*). The transient mechanism could have arisen by coupling *veg* levels to this basic transition of meristems from a newly initiated (immature) to an established (mature) state. Thus, the evolution of the transient mechanism may reflect an earlier developmental genetic constraint that biased the variants available for selection toward this mechanism (*6*).

Evolution between racemes and cymes. In uncertain or pollinator-limited environments, racemes and cymes can represent equivalent adaptive solutions separated by a valley in the fitness landscape (Fig. 5, C to E). Such low-fitness valleys may have been circumvented in various ways during evolution. One is through changes in the environment. Figure 5F shows fitness landscapes that have been calculated for different degrees of environmental uncertainty and combined to form a three-dimensional (3D) fitness space, with the vertical axis representing the standard deviation in growth duration. An inverted U-shaped high-fitness region connects racemes, panicles, and cymes. Connecting paths may also occur through variation in genetically controlled factors. For example, a path emerges when plant longevity is varied along the vertical axis (Fig. 5G). Connecting paths of this type are common features of higher dimensional genotypic spaces (*35*, *36*). We propose the general term "evolutionary wormhole" for such high-dimensional connections.

Movement along evolutionary wormholes that connect racemes and cymes appears limited, as individual genera seldom include both architectures. This constraint may arise because moving along wormholes requires coordinated changes of several parameters, involving multiple genetic steps. Large jumps between regions of high fitness are thus unlikely; moreover, gene segregation would generate low-fitness phenotypes. In addition, mutations required to move along some stretches of a wormhole, such as crossing between racemes and cymes, involve changes in regulatory interactions rather than simple loss or reduction of function. For example, creating a cyme in *Arabidopsis* would require changing the *LFY* and *TFL1* promoters or other genes that interact with *LFY*, *TFL1* or *veg,* such that *veg* becomes high in state *B* and low in state *A* (the reverse of wild type). Such mutations are likely to be rare. Thus, evolution of inflorescences is constrained by the nature of the developmental genetic mechanism, as well as by the interaction between organism and environment.

Conclusion. The diversity of inflorescence architectures reflects an interplay between development and selection at several levels. We propose that a relatively simple developmental mechanism—the transient model—underlies the restriction of inflorescence types to a small region of morphospace. This mechanism offers a selective advantage in dealing with environmental limitations and uncertainty over a simpler mechanism that can generate only panicles. Although similar advantages might also be achieved through other developmental mechanisms, the transient mechanism may have evolved because it co-opted a previously available developmental transition from the immature to mature state of apices. Within the confines of the morphospace spanned by the transient model, inflorescence architectures cannot evolve freely but are restricted to following paths of high fitness or evolutionary wormholes. The combination of theoretical and experimental approaches described here shows how development and selection can interact during evolution to carve out biological forms from the vast space of theoretical possibilities.

References and Notes

1. G. R. McGhee, *Theoretical Morphology* (Columbia Univ. Press, New York, 1999).
2. K. J. Niklas, *The Evolutionary Biology of Plants* (Univ. of Chicago Press, Chicago, 1997).
3. D. M. Raup, A. Michelson, *Science* **147**, 1294 (1965).
4. D. M. Raup, *J. Paleontol.* **41**, 43 (1967).
5. R. Raff, *The Shape of Life* (Univ. of Chicago Press, Chicago, 1966).
6. J. Maynard Smith *et al.*, *Q. Rev. Biol.* **60**, 265 (1985).
7. R. O. Erickson, F. J. Michelini, *Am. J. Bot.* **44**, 297 (1957).
8. I. M. H. Etherington, *Proc. R. Soc. Edinb.* **59**, 153 (1939).
9. W. Troll, *Die Infloreszenzen I* (Gustav Fischer Verlag, Stuttgart, Germany, 1964).
10. W. Troll, *Die Infloreszenzen II* (Gustav Fischer Verlag, Jena, Germany, 1969).
11. F. Weberling, *Morphology of Flowers and Inflorescences* (Cambridge Univ. Press, Cambridge, 1992).
12. P. Prusinkiewicz, A. Lindenmayer, *The Algorithmic Beauty of Plants* (Springer-Verlag, New York, 1990).
13. E. A. Kellogg, in *Monocots: Systematics and Evolution*, K. L. Wilson, D. A. Morrison, Eds. (CSIRO, Collingwood, Australia, 2000), pp. 84–88.
14. G. G. Simpson, C. Dean, *Science* **296**, 285 (2002).
15. T. Sachs, *Plant Cell Environ.* **22**, 757 (1999).
16. D. Barthelemy, *Acta Biotheor.* **39**, 309 (1991).
17. L. E. Gatsuk, O. V. Smirnova, L. I. Vorontsova, L. B. Zaugol'nova, L. A. Zhukova, *J. Ecol.* **68**, 675 (1980).
18. F. Parcy, K. Bomblies, D. Weigel, *Development* **129**, 2519 (2002).
19. D. Weigel, J. Alvarez, D. R. Smyth, M. F. Yanofsky, E. M. Meyerowitz, *Cell* **69**, 843 (1992).
20. E. A. Schultz, G. W. Haughn, *Development* **119**, 745 (1993).
21. D. Bradley, O. Ratcliffe, C. Vincent, R. Carpenter, E. Coen, *Science* **275**, 80 (1997).
22. O. J. Ratcliffe, D. J. Bradley, E. S. Coen, *Development* **126**, 1109 (1999).
23. S. Shannon, D. R. Meeks-Wagner, *Plant Cell* **3**, 877 (1991).
24. O. J. Ratcliffe *et al.*, *Development* **125**, 1609 (1998).
25. M. A. Blazquez, L. N. Soowal, I. Lee, D. Weigel, *Development* **124**, 3835 (1997).
26. J. Long, M. K. Barton, *Dev. Biol.* **218**, 341 (2000).
27. K. R. Hopper, T. Rosenheim, T. Prout, J. Oppenheim, *Oikos* **101**, 219 (2003).

28. D. King, J. Roughgarden, *Theor. Popul. Biol.* **21**, 194 (1982).
29. D. Cohen, *J. Theor. Biol.* **12**, 119 (1966).
30. D. King, J. Roughgarden, *Theor. Popul. Biol.* **22**, 1 (1982).
31. P. Haccou, Y. Iwasa, *Theor. Popul. Biol.* **47**, 212 (1995).
32. E. Kussell, S. Leibler, *Science* **309**, 2075 (2005).
33. L. Watson, M. J. Dallwitz, *The Families of Flowering Plants: Descriptions, Illustrations, Identification, and Information Retrieval.* Version: 29 July 2006 http://delta-intkey.com (1992 onward).
34. T. Keller, J. Abbott, T. Moritz, P. Doerner, *Plant Cell* **18**, 598 (2006).
35. A. C. Whibley *et al.*, *Science* **313**, 963 (2006).
36. S. Gavrilets, *Fitness Landscapes and the Origin of Species*, S. Levin, H. Horn, Eds., Monographs in Population Biology (Princeton Univ. Press, Princeton and Oxford, 2004).
37. We thank J. Avondo for help with visualizing 3D fitness landscapes, M. Clauss for helpful discussions on bet-hedging, and C. Thébaud for advice on inflorescence databases. This research was funded by grants from Human Frontier Science Program (E.C. and P.P.), Natural Sciences and Engineering Research Council of Canada (P.P. and L.H.), and the Biotechnology and Biological Sciences Research Council, UK (E.C.).

Supporting Online Material
www.sciencemag.org/cgi/content/full/1140429/DC1
Materials and Methods
SOM Text
Fig. S1
References
SOM Programs

25 January 2007; accepted 30 April 2007
Published online 24 May 2007;
10.1126/science.1140429
Include this information when citing this paper.

Marine Radiocarbon Evidence for the Mechanism of Deglacial Atmospheric CO_2 Rise

Thomas M. Marchitto,[1,2]*† Scott J. Lehman,[1,2]* Joseph D. Ortiz,[3] Jacqueline Flückiger,[2]‡ Alexander van Geen[4]

We reconstructed the radiocarbon activity of intermediate waters in the eastern North Pacific over the past 38,000 years. Radiocarbon activity paralleled that of the atmosphere, except during deglaciation, when intermediate-water values fell by more than 300 per mil. Such a large decrease requires a deglacial injection of very old waters from a deep-ocean carbon reservoir that was previously well isolated from the atmosphere. The timing of intermediate-water radiocarbon depletion closely matches that of atmospheric carbon dioxide rise and effectively traces the redistribution of carbon from the deep ocean to the atmosphere during deglaciation.

Radiocarbon measurements of calendrically dated hermatypic corals (*1*) and planktonic foraminifera (*2*, *3*) indicate that the radiocarbon activity ($\Delta^{14}C$) of the atmosphere during the latter part of the last glacial period [~20,000 to 40,000 years before the present (yr B.P.)] ranged from ~300 to 800 per mil (‰) higher than it was during the prenuclear modern era (Fig. 1C). Although reconstructions of Earth's geomagnetic-field intensity predict higher cosmogenic ^{14}C production rates during the glacial period, production was apparently not high enough to explain the observed atmospheric enrichment (*2*–*5*). Rather, a substantial fraction of the atmosphere's $\Delta^{14}C$ buildup must have been due to decreased uptake of ^{14}C by the deep ocean. This requires a concomitant ^{14}C depletion in a deep-ocean dissolved inorganic C reservoir that was relatively well isolated from the atmosphere. Renewed ventilation of this reservoir could theoretically explain the drop in atmospheric $\Delta^{14}C$ (Fig. 1C) and the rise in atmospheric CO_2 (*6*) across the last deglaciation. Most workers point to the Southern Ocean as a locus of deglacial CO_2 release, based on the similarity between atmospheric CO_2 and Antarctic temperature records (*6*) and on numerous conceptual and numerical models (*7*–*9*). If correct, we would expect some signature of the low-^{14}C deep-ocean C reservoir to be spread to other basins via Antarctic Intermediate Water (AAIW). Here, we report a strong radiocarbon signal of the deglacial release of old C, recorded in an intermediate-depth sediment core from the northern edge of the eastern tropical North Pacific.

Intermediate water $\Delta^{14}C$ reconstruction. Marine sediment multi-core/gravity-core/piston-core triplet from sediment layer MV99-MC19/GC31/PC08 was raised from a water depth of 705 m on the open margin off the western coast of southern Baja California (23.5°N, 111.6°W) (*10*). The site is today situated within the regional O_2 minimum zone that exists because of a combination of high export production and poor intermediate-water ventilation. Various sediment properties in MC19/GC31/PC08 vary in concert with the so-called Dansgaard-Oeschger (D-O) cycles that characterized the Northern Hemisphere climate during the last glacial period (*11*). Originally discovered in Greenland ice cores, D-O cycles also exist in a number of lower-latitude locations that were probably teleconnected to the North Atlantic region through the atmosphere (*2*, *12*, *13*). Off the coast of Baja California, the sedimentary concentrations of organic C, Cd, Mo, and benthic foraminifera all decreased sharply during D-O stadials (cold periods in Greenland) (*11*, *14*). Together, these proxies are consistent with reduced productivity during stadials, caused by either decreased coastal upwelling or a deepening of the regional nutricline related to the mean state of the tropical Pacific (*11*).

Diffuse spectral reflectance (DSR) provides a 1-cm resolution stratigraphy for GC31/PC08. After R-mode factor analysis, the third factor of DSR (Fig. 1A) exhibits the strongest correlation to the productivity proxies and to Greenland climate (*11*). We used this DSR record to apply a calendar-age model to MC19/GC31/PC08, based on correlation to $\delta^{18}O$ (an air-temperature proxy) in Greenland ice core GISP2 (Greenland Ice Sheet Project 2) (*15*). Resulting calendar ages were then combined with 50 benthic foraminiferal radiocarbon ages [19 of which were published previously (*10*)] to calculate age-corrected intermediate-water $\Delta^{14}C$ (*16*). To evaluate the partitioning of ^{14}C between the atmosphere and the ocean, we compared intermediate-water $\Delta^{14}C$ to that of the atmosphere (Fig. 1C), as reconstructed from tree rings (*17*), U-Th–dated corals (*1*, *17*), and planktonic foraminifera from Cariaco Basin off Venezuela (*3*). Calendar ages for Cariaco Basin were originally based on the correlation of lithologic climate proxies to the GISP2 $\delta^{18}O$ record (*2*), which has been layer-counted with visual and chemical techniques (*15*). However, Hughen *et al.* (*3*) recently demonstrated that the Cariaco Basin ^{14}C calibration yields much better agreement with coral results older than ~22,000 yr B.P. when an alternate age model is used, based on correlation to the U-Th–dated Hulu Cave speleothem $\delta^{18}O$ record from eastern China (*13*). Because DSR in GC31/PC08 is more similar to the Greenland isotope record than to the lower-resolution Hulu Cave record, we continued to use the GISP2 correlation but applied simple provisional age adjustments to GISP2 older than 23,400 yr B.P., using four tie points to Hulu Cave (Fig. 1B and fig. S1). We do not suggest that this age model is necessarily superior to the original one (*15*), but this exercise is necessary for comparing our data to the most recent (and most consistent) atmospheric $\Delta^{14}C$ reconstructions (*1*, *3*, *17*). The resulting age model for MC19/GC31/PC08, based on 21 tie points, yields a very constant sedimentation rate (fig. S2) and gives us confidence that our calendar-age assignments for ^{14}C samples between tie points are reliable to within a few hundred years (table S1).

Baja California intermediate-water radiocarbon activities are plotted in red in Fig. 1C. The

[1]Department of Geological Sciences, University of Colorado, Boulder, CO 80309, USA. [2]Institute of Arctic and Alpine Research, University of Colorado, Boulder, CO 80309, USA. [3]Department of Geology, Kent State University, Kent, OH 44242, USA. [4]Lamont-Doherty Earth Observatory, Columbia University, Palisades, NY 10964, USA.

*These authors contributed equally to this work.
†To whom correspondence should be addressed. E-mail: tom.marchitto@colorado.edu
‡Present address: Environmental Physics, Institute of Biochemistry and Pollutant Dynamics, Eidgenössische Technische Hochschule Zürich, 8092 Zürich, Switzerland.